biomolecules

MDPI

Article

The antioxidant drug edaravone binds to the aryl hydrocarbon receptor (AHR) and promotes the downstream signaling pathway activation

Caterina Veroni[1]*, Stefania Olla[2]*, Maria Stefania Brignone[1], Chiara Siguri[2], Alessia Formato[3], Manuela Marra[4], Rosa Manzoli[5], Maria Carla Macario[5,6], Elena Ambrosini[1], Enrico Moro[5 §] and Cristina Agresti[1§]

[1] Department of Neuroscience, Istituto Superiore di Sanità, Rome, Italy. caterina.veroni@iss.it; mariastefania.brignone@iss.it; elena.ambrosini@iss.it; cristina.agresti@iss.it
[2] Institute for Genetic and Biomedical Research (IRGB), The National Research Council (CNR), Monserrato, Cagliari, Italy. stefania.olla@irgb.cnr.it; chiara.siguri@irgb.cnr.it
[3] Institute of Biochemistry and Cell Biology, IBBC-CNR, Campus Adriano Buzzati Traverso, Monterotondo Scalo, Rome, Italy. aformato92@gmail.com
[4] Core Facilities Technical-Scientific Service, Istituto Superiore di Sanità, Rome, Italy. manuela.marra@iss.it
[5] Department of Molecular Medicine, University of Padova, Padova, Italy. rosa.manzoli@phd.unipd.it; mariacarla.macario@studenti.unipd.it; enrico.moro.1@unipd.it
[6] Department of Biology, University of Padova, Padova, Italy. mariacarla.macario@studenti.unipd.it
* Shared first authorship.
* Correspondence: Correspondence: CA cristina.agresti@iss.it, +390649903539; EM enrico.moro.1@unipd.it, +390498276341

Abstract: A considerable effort has been spent in the past decades to develop targeted therapies for the treatment of demyelinating diseases, such as multiple sclerosis (MS). Among drugs with free radical scavenging activity and oligodendrocyte protecting effects, Edaravone (Radicava) has recently received increasing attention being able to enhance remyelination in experimental *in vitro* and *in vivo* disease models. While its beneficial effects are highly supported by experimental evidence, there is currently paucity of information regarding its mechanism of action and main molecular targets. By using high-throughput RNA-seq and biochemical experiments in murine oligodendrocyte progenitors and SH-SY5Y neuroblastoma cells combined with molecular docking and molecular dynamics simulation, we here provide evidence that Edaravone triggers the activation of the aryl hydrocarbon receptor (AHR) signaling by eliciting AHR nuclear translocation and the transcriptional-mediated induction of key cytoprotective gene expression. We also show that an Edaravone-dependent AHR signaling transduction occurs in the zebrafish experimental model, associated with a downstream upregulation of the NRF2 signaling pathway. We finally demonstrate that its rapid cytoprotective and antioxidant actions boost *in vivo* increased expression of the promyelinating Olig2 transgene. We therefore shed light on a still undescribed potential mechanism of action for this drug, providing further support to its therapeutic potential in the context of debilitating demyelinating conditions.

Keywords: edaravone; aryl hydrocarbon receptor; oligodendrocyte progenitors; zebrafish

Citation: To be added by editorial staff during production.

Academic Editor: Firstname Lastname

Received: date
Revised: date
Accepted: date
Published: date

Copyright: © 2024 by the authors. Submitted for possible open access publication under the terms and conditions of the Creative Commons Attribution (CC BY) license (https://creativecommons.org/licenses/by/4.0/).

1. Introduction

The drug Edaravone (3-methyl-1-phenyl-2-pyrazolin-5-one - EDA) is a small molecule with a high lipid solubility and permeability across the blood-brain barrier that has shown promising neuroprotective activity, particularly in the context of neurological disorders characterized by oxidative stress and neuroinflammation. It was initially approved for the management of ischemic stroke in Japan and later extended to the treatment of amyotrophic lateral sclerosis in Japan, USA, Canada and Switzerland [1]. EDA has been investigated as a potential treatment in several animal models of central nervous system (CNS) disorders, like multiple sclerosis (MS) [2, 3], Parkinson's disease [4, 5], Alzheimer's disease [6] and traumatic brain injury [7]. In addition, a proof-of-concept study evaluating the protective effect of EDA in patients with early-stage Alzheimer's disease is ongoing [8].

The clinical efficacy of EDA was primarily linked to its potent scavenging activity against reactive oxygen species (ROS) [9], thus reducing oxidative tissue damage that contributes to the initiation and progression of several neurodegenerative diseases [10]. Subsequently, it was shown that EDA's neuroprotective activity is also driven by the induction of various intracellular signaling pathways. Among these, EDA has been demonstrated to activate the nuclear factor (erythroid-derived 2)-like 2 (NRF2) [2, 11-13], which regulates the expression of genes encoding phase II detoxification enzymes, contributing to the maintenance of ROS homeostasis. Evidence also shows that EDA exerts an inhibitory effect on the release of pro-inflammatory cytokines by preventing NFκB activation [14]. The neuroprotective activity of EDA has also been extensively linked to the activation of the BDNF-TrkB signaling pathway [15-18], which contributes to neuronal survival, growth and repair.

Besides its well-described neuroprotective properties, a significant amount of data provided by us and other groups has shown EDA's ability to promote remyelination, a neuroprotective, regenerative process aimed at restoring neuronal functions in demyelinating diseases, like MS. In particular, these findings demonstrate that EDA promotes the differentiation of oligodendrocytes, the myelin-forming cells of the CNS, and enhances the rate of remyelination in various *in vitro* and *in vivo* models of brain damage [3, 19, 20], also involving the mTORC1 signaling pathway [21].

The neuroprotective properties of EDA appear to be mediated through the activation of various intracellular signaling pathways, in line with the drug's multifunctional potential. However, there is currently no definitive evidence of a direct interaction between EDA and any of its potential targets. Identifying the biological targets of EDA can contribute to the development of more effective regenerative interventions and provide new insights into the molecular mechanisms of neurodegenerative diseases.

Many different technologies from a wide range of interdisciplinary fields are available to identify molecular targets of repurposed drugs. Through a computational approach, we tried to identify a potential common target/pathway that could explain the efficacy of various remyelinating drugs, including EDA [19]. Our recent findings indicated that the molecular structure of EDA is not suitable for target identification approaches involving the synthesis of tagged chemical derivatives [22]. In the present study, we employed a transcriptomics-guided drug target discovery strategy, analyzing the expression levels of genes differentially regulated in primary oligodendrocyte progenitor cells (OPCs) exposed or not to EDA, using gene expression data to identify drug-induced protein networks. We found that several transcripts related to the activation of the transcription factor aryl hydrocarbon receptor (AHR) were upregulated in OPCs treated with EDA. The next step involved the evaluation of EDA as a novel AHR agonist by docking and molecular dynamics simulations using an AHR 3D structure, the analysis of AHR nuclear translocation, and AHR target gene expression in the human neuroblastoma cell line SH-SY5Y and zebrafish larvae.

2. Materials and Methods

2.1. Animals

CD1 Swiss mice were purchased from Harlan Laboratories (San Pietro Al Natisone, Udine, Italy). The experimental procedures related to the use of CD1 Swiss mice for the establishment of cell cultures were conducted in accordance with Council Directive 86/609/EC and Decree 116/92. (Authorization n. 87/2017-PR - 09/23/2018 issued by the Service for Biotechnology and Animal Welfare of the "Istituto Superiore di Sanità" and by the Italian Ministry of Health. Zebrafish were maintained at 28°C in 5 l tanks with fish water at neutral pH, according to standard procedures (http://ZFIN.org). All procedures involving zebrafish embryos and larvae were performed according to the Italian Ministry of Health and the Local Institutional Review Board of the University of Padova (OPBA) (protocol code 312/2022-PR of 05/15/2022).

2.2. Purified OPC cultures

OPCs were obtained from neonatal mouse primary mixed glial cultures, as previously described [19, 23]. In brief, the forebrains of newborn CD1 Swiss mice were carefully freed of meninges, chopped into 0.2-mm sections and dissociated by mild trypsinization procedure and gentle mechanical disruption with a Pasteur pipette. Cells were seeded into poly-L-lysine (10 µg/ml, Merck/Sigma-Aldrich, Darmstadt, Germany) coated 60 mm diameter plastic cultured dishes (NUNC, Thermo Fisher Scientific, Waltham, Massachusetts, U.S.) at the density of 1.2×10^5 cells/cm^2 and grown at 37°C in a 91.5% air–8.5% CO2 humidified atmosphere in Dulbecco's modified eagle medium (DMEM) containing 10% Foetal Bovine Serum (FBS), 2 mM glutamine, penicillin (50 µg/ml) and streptomycin (50 µg/ml), replacing fresh medium after 1 DIV and every 2-3 days (media, sera and reagents by GIBCO, Thermo Fisher Scientific). After 8-10 days, OPCs were detached from the astroglia layer by mechanical dissociation and, to minimize contamination by microglial cells, the detached cell suspension was incubated for 1 hour at 37°C in a 175 cm^2 culture flask. The non-adhering cells were seeded in the same medium as above at the density of 1×10^5 cells/cm^2 into poly-L-lysine-coated dishes (96 well plates or in 35mm diameter plastic culture dishes in the case of MTT test and real-time RT-PCR assay, respectively). Two hours (h) after plating, the culture medium was replaced with defined serum-free DMEM without thyroid hormones [23]. Macrophage/microglia contamination accounted for less than 1% of total cells, as assessed by immunostaining with the monoclonal antibody (mAb) CD11b (AbD Serotech, Oxford, UK); glial fibrillary acid protein-positive astrocytes were virtually absent and the majority of cells (>99%) belonged to the oligodendrocyte lineage.

2.3. Transcriptome analysis

Transcriptome analysis was performed at the Next Generation Sequencing area of the Core Facilities Technical-Scientific Service, Istituto Superiore di Sanità, Rome, Italy. Primary OPCs treated with EDA (Merck/Sigma-Aldrich) 100 µM (n=4) or vehicle alone (n=4) for 16 h were used as treated and control groups, respectively. Cells were obtained from 4 independent preparations. Targeted transcriptome analysis has been performed using the Ion AmpliSeq™ Transcriptome Mouse Gene Expression Kit (Thermo Fisher Scientific), a targeted gene quantification approach that allows simultaneous gene expression measurement of more than 20,000 mouse RefSeq genes in a single assay. For library preparation, a barcoded cDNA library is first generated with SuperScript® VILO™ (Invitrogen, Thermo Fisher Scientific) cDNA Synthesis kit from 10ng of total RNA. Then cDNA is amplified using Ion AmpliSeq™ technology to accurately maintain expression levels of all targeted genes. Amplified cDNA Libraries were evaluated for quality and quantified using a Bioanalyzer High sensitivity chip

(Agilent, Santa Clara, U.S.). Libraries were then diluted to 100pM and pooled equally, with eight individual samples per pool. Pooled libraries were amplified using emulsion PCR on Ion Torrent OneTouch2 instruments (OT2) and enriched following the manufacturer's instructions. Templated libraries were then sequenced on the Ion GeneStudio™ S5 System. AmpliSeq sequencing data were analyzed using the Torrent Suite software and were normalized using reads per million (RPM). Both Differential Gene Expression Analysis and Principal Component Analysis were performed using the Transcriptome Analysis Console (TAC, Thermo Fisher Scientific). Genes showing differential regulation of ± 1.5 and a p-value < 0.05 (with ANOVA test) in treated cells compared to control cells were considered for further analysis.

2.4. RNA extraction and quantitative (q)PCR

Total RNA was extracted by OPCs, SH-SY5Y cells and zebrafish larvae using a RNeasy mini kit (Qiagen, Redwood City, CA, U.S.) including a DNase digestion step to eliminate genomic DNA. Five hundred nanograms of RNA were then reverse transcribed using the High Capacity Reverse Transcription kit (Thermo Fisher Scientific). Gene expression analysis has been performed by qPCR using the ABI PRISM 7500 System (Applied Biosystem, Thermo Fisher Scientific), using the TaqMan Gene ExpressionMaster Mix (Thermo Fisher Scientific) and inventoried FAM-labeled gene expression assays (Thermo Fisher Scientific) listed in Table S1 GAPDH was used as a housekeeping gene in all experimental systems (OPCs, SH-SY5Y cells, zebrafish larvae). Gene expression levels were calculated using the formula $2^{-\Delta Ct}$ or $2^{-\Delta\Delta Ct}$, where ΔCt is the difference in cycle threshold between target cDNA and housekeeping cDNA and ΔΔCt is the difference between ΔCt of treated cells/larvae and ΔCt of untreated samples.

2.5. Preparation of proteins for docking

The X-ray crystallographic structures of AHR were retrieved from the protein data bank (https://www.rcsb.org/), with accession ID 7ZUB [24]. The protein preparation wizard (Schrödinger Suite Release 2022–3) was used to prepare the protein. The bond orders were assigned, and possible missing hydrogen atoms in the 3D structure were added. Epik (Schrödinger Suite Release 2022–3) was employed to generate the heteroatoms' states at pH 7,4 ± 2,0. Full energetic optimization was performed in the final refinement step using the OPLS4 force field and the RMSD of heavy atoms was set at 0.3 Å [25].

2.6. Preparation of ligands for docking

The structures of all ligands were prepared with LigPrep (Schrödinger Suite Release 2022-3) using the OPLS4 force field, generating the possible ionization states at pH 7.0 ± 2.0, and retaining the specified chirality.

2.7. Docking studies

The 3D structure includes AHR-HSP90-XAP2, with the ligand indirubin (INDI) bound to the PSA-B domain of AHR [24]. Docking was performed on the entire protein and focused on the INDI binding site. The Receptor Grid Generator was employed to generate suitable grids for the docking with Glide [26, 27]. Two grids were generated, one encompassing the entire protein domain, while the other, with more restricted dimensions of 46 × 46 × 46 Å, utilized the INDI center in the domain as its grid center and the chosen force field was OPLS_2005 [28]. Glide-XP (Schrödinger Suite Release 2022-3) [26, 27, 29] was chosen as one of the docking protocols. Three poses per ligand were kept during the post-docking minimization using a threshold of 0.50 kcal/mol and, also in this case, the OPLS_2005 was used as the force field. The results from docking were then submitted to MM-GBSA (Molecular Mechanics with Generalized

Born and Surface Area solvation) [30] using VSGB as the solvation model and OPLS4 as the force field [31]. Using AutoDock software [32], Gasteiger charges [33] were assigned to the protein structure and again two grids were generated with AutoGrid [34]. The established dimensions were 50 × 50 × 50 Å entered within the binding site for the focused one, while the other encompassed the entire protein (blind). Docking experiments were performed using the genetic algorithm [35, 36] with 250 trials and a population of 500 individuals. The maximum number of generations and evaluations was set to 10.000.000 and 25.000.000, respectively. The other parameters were kept as defaults.

2.8. Molecular Dynamics

Molecular Dynamics (MD) simulations were performed using Desmond (Schrödinger Suite Release 2022-3) [37] and the TIP3P solvent model [38] was employed. The ligand-receptor complex was placed in an orthorhombic water box, which extended 10.0 Å, and the box volumes were minimized and neutralized by adding ions (Na+ or Cl-). The OPLS4 force field was chosen. MD simulations were conducted for a duration of 500 ns in the NPT ensemble, with the maintenance of a constant temperature (300.0 K) using the Nosé-Hoover thermostat [39], while the Martyna-Tobias-Klein barostat method [40] was used for the pressure (1.01325 bar). Generated trajectories were subjected to clustering based on RMSD using Schrödinger's trj_cluster.py script [41] and subsequently analyzed through MMGBSA analysis using the thermal mmgbsa.py script integrated within Desmond [37].

2.9. SH-SY5Y cell cultures and treatments

The SH-SY5Y cell line was kindly provided by Dr. Cinzia Mallozzi (ISS, Rome Italy) [42], and maintained in culture in Dulbecco's modified Eagle medium (DMEM)/nutrient mixture F-12 (Sigma-Aldrich, St. Louis, MO), supplemented with 10% FBS (GIBCO Life Technologies, Grand Island, NY), 1% Glutamine, 1%, Penicillin-Streptomycin (Sigma-Aldrich, St. Louis, MO) at 37° C in a humidified incubator with 5% CO2. To study AHR nuclear translocation, cells were plated in 100 mm diameter dishes ($1x10^6$ cells), maintained in culture conditions for 48 h, and stimulated for different time lengths [15 minutes (min), 30 min, 2 h, 6 h] with 100 μM of EDA (Merk/Sigma-Aldrich) or INDI, (Merck/Sigma-Aldrich) 1μM. For CYP1a1 and NRF2 protein expression analysis, cells were treated for 24 h with EDA 100 μM or INDI 1μM. To inhibit the AHR nuclear translocation, cells were treated with 1μM AHR antagonist III GNF351 (Merck/Sigma-Aldrich) for 15 min before the addition of EDA or vehicle alone (DMSO).

2.10. Protein extract preparation and western blotting

Cytosolic and nuclear protein extracts from SH-SY5Y cell line untreated or treated for AHR nuclear translocation or AHR inhibition experiments were obtained using a Nuclear extraction kit (#ab113474; Abcam), as outlined in the manufacturer's protocol. Briefly, cell samples were washed in ice-cold phosphate-buffered saline (PBS) and centrifuged for 5 min at 1,000 rpm. Then, cells were resuspended in an extraction buffer on ice for 10 min and centrifuged for 1 min at 12,000 rpm. After centrifugation, the cytosolic and nuclear fractions were collected and stored at -80°C for western blot analysis. Quantification of protein loading content was carried out using a bicinchoninic acid assay (BCA) protein assay kit (Thermo Fisher Scientific). Equal amounts of proteins (40 μg) were resolved on SDS–PAGE using gradient (4–12%) pre-casted gels (Invitrogen, ThermoFisher Scientific) and transferred onto a nitrocellulose membrane using the Trans-Blot Turbo Transfer System (BioRad, Hercules, CA, USA). Nitrocellulose membranes were blotted overnight (ON) at 4°C using anti-AHR mAb (1:1000, Santa Cruz Biotechnology), anti-CYP1A1 mAb (1:200, Santa Cruz

Biotechnology), anti-NRF2 mAb 1:500 (Santa Cruz Biotechnology), anti-GAPDH mAb (1:1000, Santa Cruz Biotechnology), anti-Actin mAb (1:2000, Santa Cruz Biotechnology). anti-Lamin B1 mAb (1:1000, Santa Cruz Biotechnology). After washings in Tris-buffered saline (TBS), membranes were incubated with horseradish peroxidase-conjugated anti-mouse Ab (1:5000; BioRad Laboratories) for 1 h at RT. Immunoreactive bands were visualized using an enhanced chemiluminescence reagent (Thermo Fisher Scientific) and exposed on a BioRad ChemiDoc XRS system. Densitometric analyses of Western Blot experiments were performed using NIH ImageJ software (https://imagej.net/ij/) or BioRad ChemiDoc XRS system.

2.11. Drug treatments on fish

Wild-type and transgenic embryos were subjected to drug exposure at 8 hours post-fertilization (hpf). The chorion of each single embryo was manually perforated with a small needle before exposure to each treatment. EDA and GNF351 were dissolved in fish water at the reported concentrations, changing the medium after 24 h in the two-day treatments. After the treatments, larvae were euthanized with an overdose of Tricaine and their trunks were manually dissected using needles. After several washes in PBS, pooled trunk tissues were solubilized in Tissue Extraction Buffer (Thermofisher, Italy) added with Protease and Phosphatase Inhibitors (Thermofisher, Italy). For fish transiently expressing the XRE-reporter transgene we first removed the luciferase coding sequence from the PXRE3G5-FL plasmid [43] and cloned the EGFP coding sequence by HindIII and EcoRI digestion and ligation. We next microinjected one-cell stage embryos with 500 pg/embryo and proceeded with the treatment as described above.

2.12. Statistical analysis

Statistical analyses were performed using IBM SPSS statistics 26.0 software. A two-way ANOVA test for repeated measures was applied for comparisons over time, while paired Student's t-test was used for comparisons between two groups. Results are expressed as mean ± standard error of the mean (SEM). p values of less than 0.05 were considered statistically significant and are expressed as * for $p < 0.05$, ** for $p < 0.01$ and *** for $p < 0.001$.

3. Results

3.1. Edaravone increases the expression of AHR-related target genes in primary mouse OPCs

Targeted transcriptome analysis was performed to analyze genes and pathways that were differentially regulated in primary OPCs with or without EDA treatment (100 μM, 14 h). The incubation period was chosen based on the results obtained in preliminary experiments, which showed that shorter incubation times (2-8 h) were not sufficient to induce a substantial modulation of gene expression. As shown in Figure 1, 1132 genes were significantly modulated by EDA treatment compared to control samples (ANOVA, $p<0.05$).

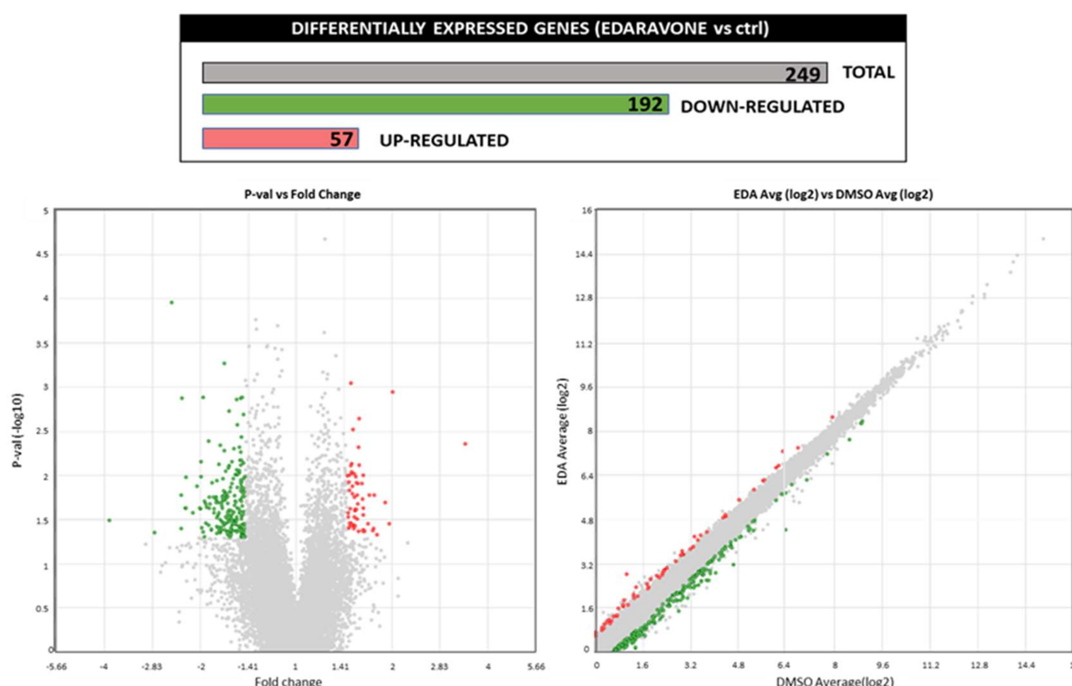

Figure 1. Effect of EDA treatment on OPC transcriptome. Purified OPCs were incubated with EDA 100 µM or vehicle alone (DMSO) for 14h. RNA was extracted, reverse transcribed and subjected to targeted transcriptome analysis. Treatment with EDA regulated the expression of 249 genes ranging in ± 1.5 fold-change with a P-value < 0.05. The Volcano plot shows statistical significance (P-value) versus magnitude of change (fold change); red and green dots represent the up- and down-regulated genes, respectively. The image was edited using BioRender.com.

Among these, 249 genes with a fold change ranging between ± 1.5-fold of the mean reads assigned per million mapped reads (RPM) values between EDA-treated and control samples were selected for further analysis. Raw transcriptomics data are supplied as supplementary material (Spreadsheet S1). Gene function was assigned using the Database for Annotation, Visualization and Integrated Discovery (DAVID, NIH) [http://david.abcc.ncifcrf.gov/]. Table 1 displays the functional classification of the significantly up-regulated (n=57) and down-regulated (n=192) genes in biological pathways.

Table 1. Biological pathways most significantly modulated by Edaravone treatment in OPCs.

	Category	Term	Count	%	p-value
UP-REGULATED	REACTOME_PATHWAY	Cytochrome P450 - arranged by substrate type	3	5,5	1,1E-2
	REACTOME_PATHWAY	Synthesis of epoxy (EET) and dihydroxyeicosatrienoic acids (DHET)	2	3,6	1,5E-2
	REACTOME_PATHWAY	Synthesis of (16-20)-hydroxyeicosatetraenoic acids (HETE)	2	3,6	1,8E-2
	REACTOME_PATHWAY	Phase I - Functionalization of compounds	3	5,5	2,3E-2
DOWN-REGULATED	KEGG_PATHWAY	Phagosome	5	2,9	4,7E-2
	KEGG_PATHWAY	PI3K-Akt signaling pathway	7	4,1	5 E-2
	REACTOME_PATHWAY	Mitotic Prometaphase	8	4,7	1,3E-3
	REACTOME_PATHWAY	Metabolism of water-soluble vitamins and cofactors	5	2,9	1,4E-2
	REACTOME_PATHWAY	Metabolism of vitamins and cofactors	6	3,5	1,5E-2

REACTOME_PATHWAY	Nucleotide catabolism	3	1,7	3,8E-2
REACTOME_PATHWAY	Organelle biogenesis and maintenance	6	3,5	4,5E-2
REACTOME_PATHWAY	M Phase	8	4,7	4,9E-2
WIKIPATHWAYS	Translation factors	4	2,3	6,4E-3
WIKIPATHWAYS	Focal adhesion: PI3K-Akt-mTOR signaling pathway	7	4,1	3,7E-2

The analysis revealed that EDA treatment significantly enhanced the expression of three genes involved in cytochrome p450 (CYP) activity: aryl-hydrocarbon receptor repressor (*Ahrr*), cytochrome P450 family 1 subfamily A member 1 (*Cyp1a1*) and B member 1 (*Cyp1b1*). All these genes are known key targets of the AHR pathway, being *Cyp1a* and *Cyp1b* involved in the cellular detoxification response [44]. We validated this finding through additional experiments performed by qPCR, which demonstrated a significant increase in the expression levels of *Ahrr*, *Cyp1a1* and *Cyp1b1* after treatment of OPCs with EDA at concentrations of 30 μM and 100 μM (Figure 2).

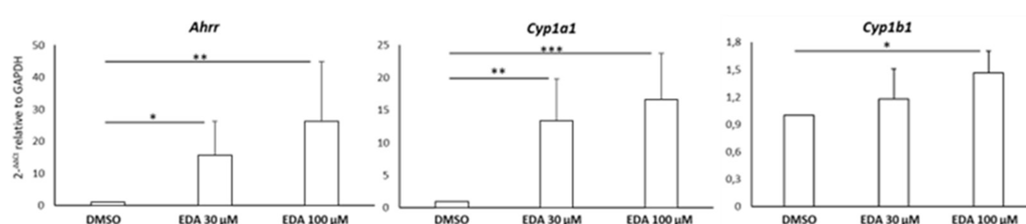

Figure 2. Validation of the effect of EDA treatment on AHR-related transcript expression in OPCs. OPCs were treated with EDA 30μM, 100 μM or vehicle (DMSO) alone for 14h. Total RNA was extracted and reverse transcribed and the expression of the selected genes was evaluated using qPCR. Data are expressed as $2^{-\Delta\Delta Ct}$ relative to the housekeeping gene *Gapdh*. Bars represent the mean ±SEM of 5 independent experiments. *p<0.05, **p<0.01, ***p<0.001 with paired Student's T-test. The image was edited using BioRender.com.

Collectively, we could infer that among different primary targets, EDA is responsible for AHR pathway activation in mouse OPCs.

3.2. Edaravone is predicted to be an AHR ligand

To verify the hypothesis that EDA activates the AHR signaling pathway by directly binding to AHR, we investigated the potential binding mode through docking studies, using INDI and leflunomide, known AHR agonists, as reference compounds. The AutoDock and Glide software tools [29, 32] were used to carry out both focused and blind docking for all compounds, leveraging the Cryo-EM structure that was recently published [24]. Next, the best docking poses of Glide complexes were chosen to perform binding energy calculations using the MM-GBSA protocol. The MM-GBSA rescoring analysis was carried out to eliminate false positive predictions. The results of these analyses consistently indicated that EDA, along with the two reference compounds, binds to AHR at the same site as the complexed INDI (Figure 3).

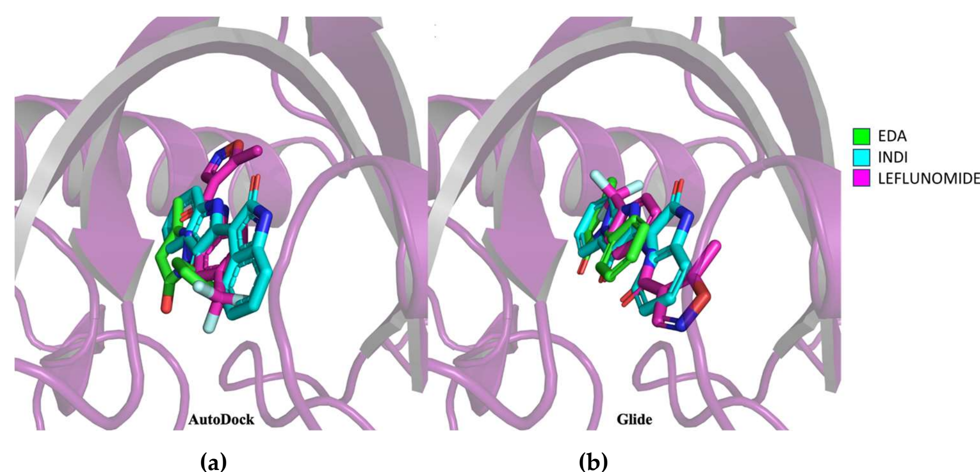

(a) **(b)**

Figure 3. Prediction of EDA–AHR binding mode by molecular docking. (a) Superimposition of docking results on AHR of EDA in green, INDI in cyan and leflunomide in magenta using Autodock software. (b) Superimposition of docking results on AHR of EDA in green, INDI in cyan and leflunomide in magenta using Glide software. The image was edited using BioRender.com.

In particular, the two software tools identified identical orientations for INDI and EDA, except for the orientation of the benzene ring in EDA. In contrast, the two software poses of leflunomide docked it within the binding pocket, but with different orientations. As shown in Table 2, EDA exhibits higher docking energies (-7.55 kcal/mol Glide and -5.97 kcal/mol AutoDock) and binding free energy (dG bind, -45.03 kcal/mol) compared to the two agonists, yet still within satisfactory ranges.

Table 2. Scores obtained from the different docking tools.

Compound	XP-GScore Glide XP Kcal/mol	MMGBSA_dGbind Prime Kcal/mol	Binding Energy (BE) Autodock Kcal/mol
Indirubin	-11.33	-67.57	-9.08
Leflunomide	-9.074	-51.34	-7.17
Edaravone	-7.55	-45.03	-5.97

To assess the stability of the AHR-EDA complex, a MD study was conducted for 500 ns, employing the docking-derived binding pose from the Glide software as the starting input. The dynamics confirmed the binding between EDA and AHR but unveiled that EDA frequently undergoes binding transitions within the pocket shifting slightly from the binding identified by docking (Figure S1).

3.3. Edaravone induces AHR nuclear translocation and AHR target gene expression in the SH-SY5Y neuroblastoma cell line

To validate the docking prediction and assess whether EDA-mediated AHR pathway induction could be conserved in a human experimental model, we assessed the ability of EDA to induce nuclear translocation of AHR and subsequent expression of endogenous AHR target genes in the neuroblastoma cell line SH-SY5Y, which represents a relevant cellular model for investigating this signaling pathway [45]. Cells were treated with EDA 100 μM for 15 min, 30 min, 2 h and 6 h. Cell lysates were then collected and subjected to fractionation into cytosolic and nuclear fractions. Western Blot results showed that AHR protein levels significantly decreased in cytosolic-containing fractions within 2 h of EDA treatment, while increasing AHR protein levels were detected in the nuclear fractions over 6 h of EDA treatment (Figure 4).

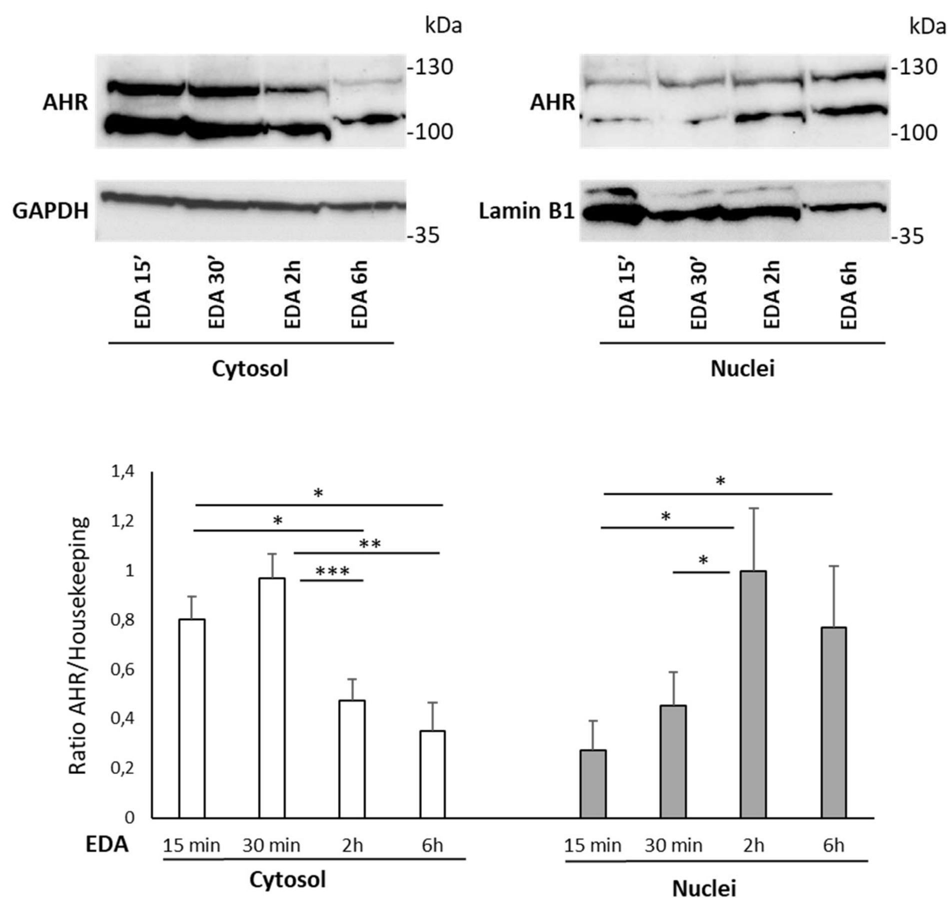

356

Figure 4. EDA induction of AHR nuclear translocation in SH-SY5Y neuroblastoma cell line. SH-SY5Y human neuroblastoma cells were incubated with EDA 100 μM for 15 min, 30 min, 2h and 6h. The cytosolic and nuclear fractions were separated and the expression level of AHR in each fraction was evaluated by Western Blot analysis. GAPDH and LAMINB1 were used for protein content normalization in cytosol and nuclei, respectively. Bars represent the mean ±SEM of 4 experiments. *$p<0.05$, **$p<0.01$, ***$p<0.001$ with 2-way ANOVA analysis for repeated measures. The image was edited using BioRender.com. 357 358 359 360 361 362 363 364

In addition, the expression of *AHRR* and *CYP1A1* genes was examined at both transcript and protein levels. SH-SY5Y cells were incubated with EDA 30 and 100 μM for 14 h, using INDI, the known AHR endogenous ligand, as positive control.

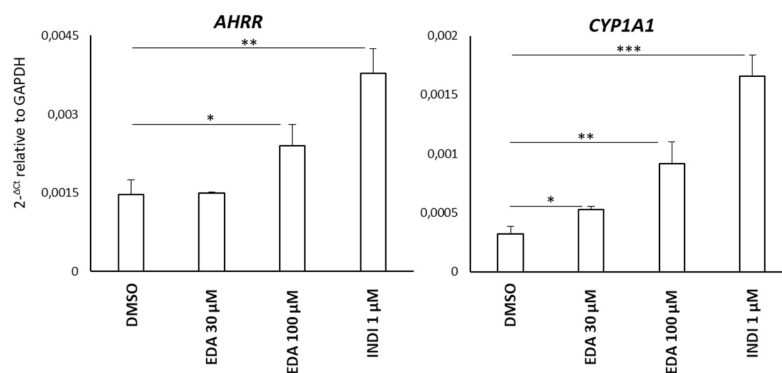

(**a**)

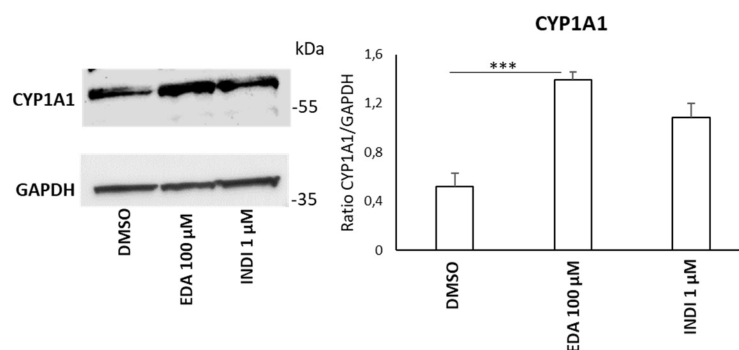

(**b**)

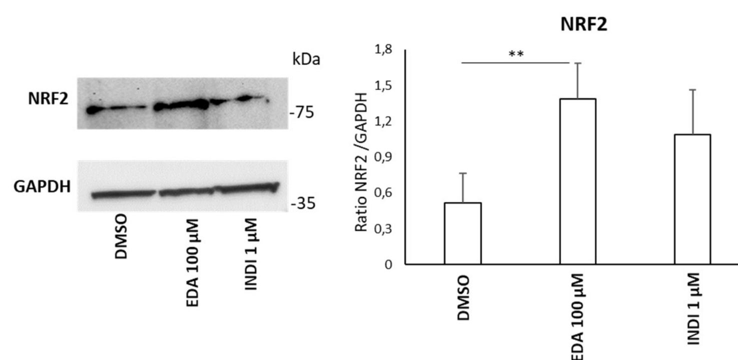

(**c**)

Figure 5. EDA-induction of AHR target genes in SH-SY5Y neuroblastoma cell line. (a). SH-SY5Y cells were incubated with EDA 30 μM, EDA 100 μM, INDI 1 μM or DMSO alone for 14h. Total RNA was extracted and the expression of *AHRR* and *CYP1A1* transcripts was evaluated using qPCR. Data are expressed as $2^{-\Delta Ct}$ relative to the housekeeping gene *GAPDH.* (b,c). SH-SY5Y cells were treated with EDA 100 μM, INDI 1 μM or DMSO alone for 24h and CYP1A1 (b) and NRF2 (c) protein expression was investigated by Western Blot. Data are expressed as the ratio between AHR and GAPDH reference. Bars represent the mean ±SEM of 3 experiments. *$p<0.05$, **$p<0.01$, ***$p<0.001$ using paired Student's T-test. The image was edited using BioRender.com.

EDA significantly increased *AHRR* and *CYP1A1* transcript levels (Figure 5a), as well as CYP1A1 protein levels (Figure 5b). As NRF2 is a key downstream target of AHR [46], we next evaluated EDA activity on *NRF2* expression in our experimental model. Western Blot data showed a significant up-regulation of NRF2 in the nuclear fraction after treatment of SH-SY5Y with EDA at a concentration of 100 μM for 24 hours compared to unstimulated cells (Figure 5c). Our findings demonstrated that, in response to EDA, AHR is activated and translocates from the cytoplasm to the nucleus, where it induces the expression of its target genes.

3.4. Edaravone promotes AHR and NRF2 pathways activation and Olig2 transgene expression in zebrafish larvae

To confirm EDA activity on the AHR pathway in an *in vivo* model, we measured the expression levels of the *cyp1a1* zebrafish orthologue in EDA-treated larvae. Eight hpf embryos were exposed to EDA at 10 and 30 μM or DMSO for 24 and 48 h and *cyp1a* transcript levels were determined by qPCR. As shown in Figure 6a, EDA induced a significant up-regulation of *cyp1a* in treated larvae. To further confirm that EDA was specifically inducing the AHR pathway at a transcriptional level, we transiently overexpressed a plasmid containing three xenobiotic responsive elements (XRE) upstream of the eGFP coding sequence [43].

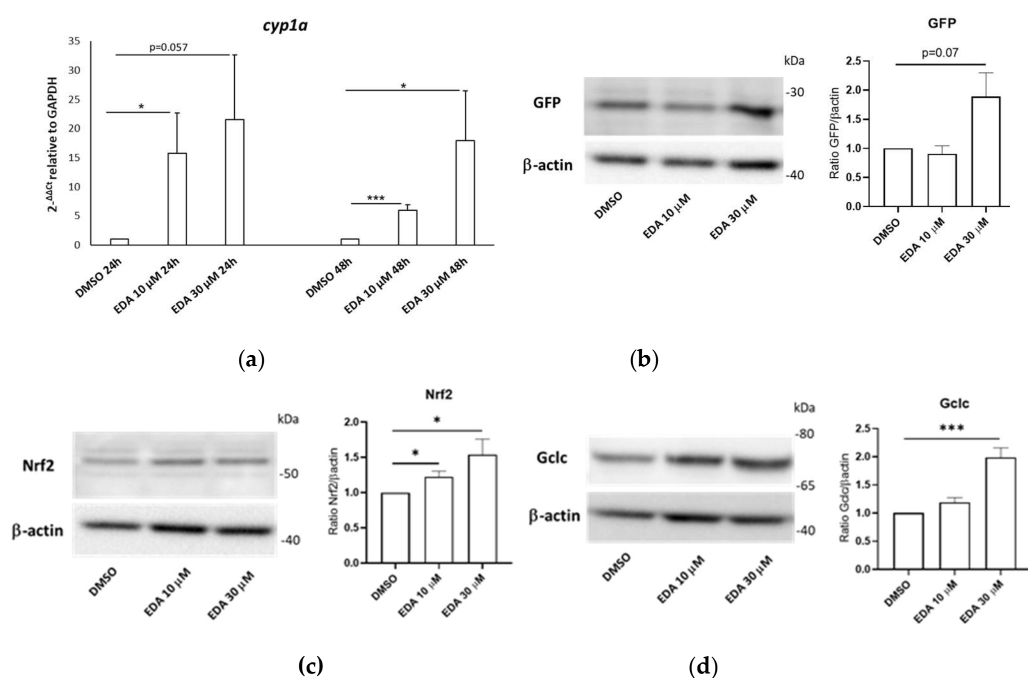

(a) (b)

(c) (d)

Figure 6. EDA promotes AHR and NRF2 pathway activation in zebrafish larvae. (a) *cyp1a* transcript expression in zebrafish larvae at 56 hpf treated with vehicle (DMSO), EDA 10 and 30 μM, for 24 and 48 h. (b) Representative Western Blot for the eGFP reporter protein on fish trunk whole lysates from control DMSO and EDA-treated *Tg(8x AORE:EGFP)^{ia201}* larvae at 56 hpf. Fish were treated for 48 consecutive hours. For both gene expression and Western Blot analysis, data are expressed as the mean ±SEM of 4 biological replicates (10 larvae per replicate). (c, d). Representative Western Blot for Nrf2 and Gclc proteins on fish trunk whole lysates from control DMSO and EDA-treated larvae at 56 hpf. Data are expressed as the mean ±SEM of 6 biological replicates (10 larvae per replicate). *$p<0.05$, ***$p<0.001$ with paired Student's T-test. The image was edited using BioRender.com.

Treatment of fish embryos transiently expressing the reporter cassette at 8 hpf with EDA (30 μM) for 24 hours led to increased GFP fluorescence (Figure S2).

To further investigate and corroborate the antioxidant response elicited *in vivo* by EDA, we first treated a recently generated Nrf2 pathway reporter fish [47] with EDA for 48 h and evaluated by Western Blot the expression levels of the reporter gene (GFP). Compared to age-matched DMSO-treated fish, EDA-treated fish exhibited higher, although at the margin of statistical significance ($p=0.07$), GFP protein levels when compared to control fish (Figure 6b). We next evaluated in the same EDA-treated fish and DMSO controls the expression levels of the transcription factor Nrf2 and the glutamate cysteine ligase catalytic subunit (Gclc), which is the rate-limiting enzyme in the synthesis of glutathione and a NRF2 downstream target [48]. As shown in Figure 6 (c, d), both Nrf2 and Gclc protein levels were significantly upregulated in EDA-treated fish when compared to age-matched controls. As accumulating evidence indicates that AHR and NRF2 are involved in oligodendrocyte development and myelination processes [49, 50], we also analyzed the effects of EDA on the induction of oligodendrocyte lineage specification using the previously described *Tg(Olig2:eGFP)^{vu12}* line [51].

As shown in Figure 7, treatment of 8 hpf *Tg(Olig2:eGFP)^{vu12}* transgenic fish with 30 µM EDA for 48 hours induced a significant increase in reporter protein expression (GFP). Collectively, these results confirmed that EDA treatment triggers *in vivo* the activation of the AHR and NRF2 signaling axis and fosters Olig2+ oligodendrocyte lineage expansion.

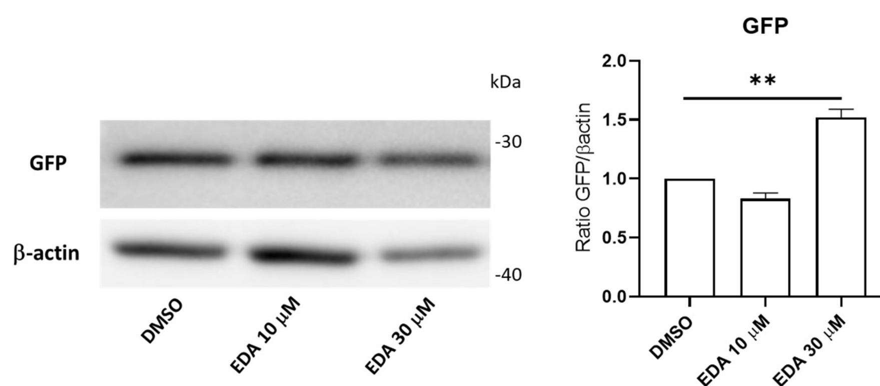

Figure 7. EDA treatment induces reporter expression in Olig2 transgenic fish. Representative Western Blot for the eGFP reporter protein on fish trunk whole lysates from control DMSO and EDA-treated *Tg(Olig2:eGFP)^{vu12}* transgenic fish. Data are expressed as the mean ±SEM of 3 biological replicates (10 larvae per replicate). **$p<0.01$ with paired Student's T-test. The image was edited using BioRender.com.

3.5. Edaravone-mediated induction of CYP genes is dampened by the AHR antagonist GNF-351 in SH-SY5Y cells and zebrafish

We next verified whether the up-regulation of genes associated with the AHR pathway could be prevented by the administration of the competitive AHR antagonist GNF-351, which exhibits effective antagonism against a wide range of AHR ligands [52]. SH-SY5Y cells were treated with EDA (30 µM and 100 µM) in the presence or absence of the GNF-351 1µM for 14 h. The dose of 1µM was selected based on preliminary dose-response experiments (data not shown). As shown in Figure 8a, co-treatment with GNF-351 completely prevented the EDA-dependent increase of *AHRR* and *CYP1A1* transcript levels. In agreement with these observations, we also co-treated fish larvae with 30 µM EDA and 5 µM GNF-351 for 24 h and evaluated the expression levels of the target genes *cyp1a* and *ahrr*. Figure 8b shows that inhibition of AHR by GNF-351 was able to prevent the EDA-dependent upregulation of the target genes

cyp1a and *ahrr*. Based on these findings, we can state that the upregulation of AHR target genes is directly mediated by the impact of EDA on AHR activity.

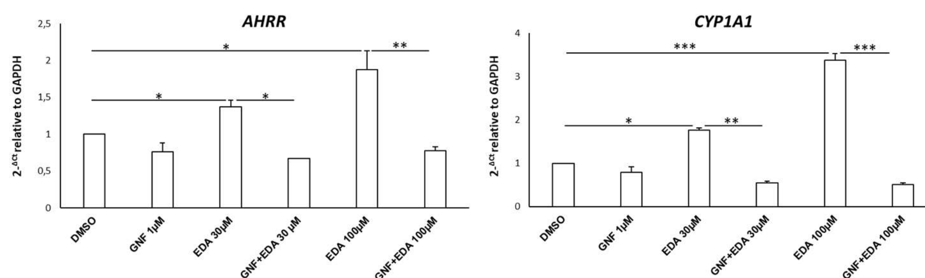

(**a**)

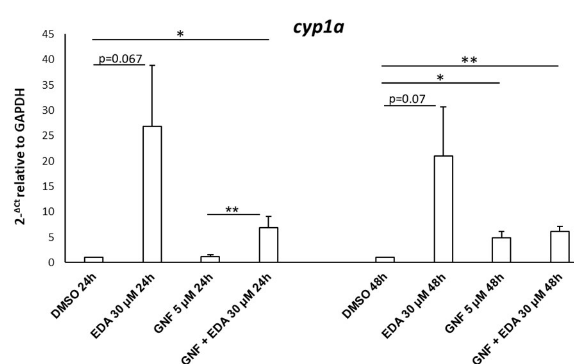

(**b**)

Figure 8. AHR inhibition curtails EDA-mediated AHR target genes upregulation *in vitro* and *in vivo*. Bar graphs show the gene expression levels detected by qPCR on RNA obtained from SH-SY5Y cells (a) and zebrafish larvae (b). Cells were treated with DMSO, EDA 30 µM and 100 µM and/or GNF-351 1 µM for 24 h. B. Zebrafish larvae at 8 hpf were treated with DMSO, EDA 30 µM in the presence or absence of GNF-351 1µM for 24 h and 48 h. The mean ±SEM of 3 experiments is shown. ***$p<0.05$, **$p<0.01$ *** $p<0.001$ with paired Student's T-test. The image was edited using BioRender.com.

3.6. GNF-351 competes for the same AHR binding site with Edaravone

Next, we wanted to assess whether EDA and GNF-351 can efficiently and directly interact with the same ligand binding pocket of AHR through docking and molecular dynamics studies. Both AutoDock and Glide confirmed binding of GNF-351 in the same pocket of EDA, but with a lower energy (-8.16 kcal/mol and -10.55 kcal/mol, respectively), confirming the higher activity and affinity of the antagonist. The two software identified similar interactions, including pi-pi stacking with His 291 and Phe 324, aromatic H-bond with Ser 346 and pi-pi stacking with Phe 295 for AutoDock and aromatic H-bond with Ser 320 for Glide (Figure S3). To assess binding stability, MD was performed, confirming GNF-351's stable binding to AHR. Throughout more than 30% of dynamics, H-bond interactions were observed with Ser 365 (95%), Phe 295 (42%) and Tyr 322 (30%), along with pi-pi stacking with Tyr 322 (76%), Phe 295 (50%) and His 291 (34%) (Figure S4). During simulation GNF-351 exhibits stabilization within the pocket and undergoes movement relative to the identified docking (Figure S5). The average MMGBSA calculation throughout the dynamic is -95.209 ± 5.106 kcal/mol, once more demonstrating a lower value compared to EDA. This further confirms the higher affinity of GNF-351 for AHR within the identical pocket occupied by EDA.

4. Discussion

EDA is a free radical scavenger and antioxidant agent with neuroprotective and remyelinating properties. Uncovering direct molecular targets that mediate its biological activity is critical to understanding the full therapeutic potential of the drug.

By performing *in vitro*, *in vivo* and *in silico* experiments, our current study establishes that EDA is a novel agonist of the transcription factor AHR and induces an AHR-dependent expression of known target genes.

AHR was first characterized as a ligand-induced transcriptional regulator involved in the adaptive response for xenobiotic detoxification [53]. Accumulating evidence strongly supports AHR's relevant role in an array of physiological processes, like cellular homeostasis, cell development and immune response [54]. AHR is activated by environmental contaminants, naturally occurring compounds and endogenous metabolites. Following ligand binding, AHR translocates into the nucleus, forms a dimer with the nuclear translocator ARNT and stimulates the transcription of target genes carrying xenobiotic responsive elements (XREs) in the promoter region, such as CYP1 family genes and the repressor AHRR, which counteracts AHR-dependent gene expression.

Using targeted transcriptomic analysis and qPCR, we observed a significant increase in the expression of genes related to the AHR pathway (*CYP1A1, CYP1B1, AHRR*) in mouse OPCs and human neuroblastoma SH-SY5Y cells after treatment with EDA. Additionally, we showed that EDA was able to promote the expression of AHR target genes and induce reporter activity in transient XRE:eGFP overexpressing zebrafish larvae.

CYP1A1 gene expression is primarily regulated by the AHR, thus establishing this gene as a distinctive marker of AHR pathway activation [55]. The complete inhibition of *CYP1A1* induction in neuroblastoma cells and *cyp1a* in zebrafish by the AHR antagonist GNF-351 strongly supports the hypothesis that AHR activation is instrumental for EDA-induced CYP pathway stimulation.

In support of the assumption that EDA acts as an AHR ligand, our *in silico* studies predicted a favorable and stable energy profile of the drug within the binding pocket over time. The evidence that EDA and GNF-351 bind to the same AHR pocket suggests a competitive antagonism between the two ligands. Notably, GNF-351 has an advantage in this competition due to its higher binding affinity compared to EDA, as also pointed out. The finding that EDA promoted AHR nuclear translocation in SH-SY5Y cells reinforces the idea that AHR activation may occur in the presence of direct ligand binding, excluding non-genomic mechanisms previously reported for some compounds in the activation of AHR target genes [56].

Our research also showed that EDA effectively enhances *NRF2* expression in both SH-SY5Y cells and zebrafish larvae. This result supports the involvement of NRF2 signaling in the drug's antioxidant activity, as previously demonstrated in various models of neurodegenerative diseases [2, 11- 13]. Given that *NRF2* is a target gene of AHR, bearing at least one functional XRE sequence in its promoter [46], and is also activated through ROS generated by CYP1A1 [57], we postulate that EDA's activity is possibly mediated through the AHR- NRF2 pathway. The complex crosstalk between these two signaling pathways leads to the induction of cytoprotective genes encoding detoxificating and antioxidant enzymes that may explain many of the effects already described for the drug [58].

We observed that EDA activates the AHR pathway during the differentiation of purified mouse OPCs *in vitro* and in developmental oligodendrogenesis in zebrafish (24-56 hpf). We also showed that in zebrafish larvae EDA not only activates the AHR-NRF2 pathway but also increases *Olig2* transgene expression. This aligns with recent findings indicating that proper modulation of the AHR signal is essential for oligodendrocyte development in zebrafish models [59], although, at odds with this work, we found that AHR- NRF2 pathway activation by EDA increases reporter expression in the *Olig2:GFP* transgenic line. The apparent contrasting effects reported

by Martins and colleagues on AHR pathway induction and oligodendrogenesis may be ascribed to additional secondary effects produced by tetrachlorodibenzo-para-dioxin when compared to those of EDA. Alternatively, underexplored mechanisms of EDA action may be dominant over the previously described negative effect of AHR activation on the oligodendroglial population expansion. To support the first scenario, the key role of AHR in oligodendrocyte differentiation and myelination was already elucidated through the analysis of AHR knockout models [49, 60] and subsequently strengthened by the finding that AHR activation increases sphingolipid levels and axon myelination [61]. Therefore, the combination of our data with evidence from the literature leads us to suggest AHR as the target responsible for the pro-myelinating effect of EDA [3, 19-21] likely due to the expansion of the oligodendroglial lineage. 544 545 546 547 548 549 550 551 552 553 554

Ensuring the proper modulation of AHR signaling is crucial for maintaining cellular homeostasis. The inactivation or overactivation of the AHR pathway has been demonstrated to contribute to the dysregulation of proinflammatory and neurodegenerative mechanisms in several neurological diseases [62]. Notably, a recent study by Tsaktanis et al. [63] found a decrease in AHR agonistic activity in the serum of MS patients, showing a correlation with disease progression. 555 556 557 558 559 560

EDA, along with other drugs already in use in the clinic [64, 65], emerges as an ideal AHR agonist, as it triggers the favorable aspects of AHR activation without the undesired side effects observed with dioxin-like chemical pollutant derivatives. While recognizing the need for further studies to establish the mechanistic link between AHR activation and NRF2 pathway induction, as well as its correlation with increased expression of the downstream *Olig2* transgene, we envisage that the identification of AHR as a key molecular target of EDA will pave the way for more informed design of new molecules with improved AHR binding activity and affinity, which might be considered for the screening of pro-myelinating compounds. 561 562 563 564 565 566 567 568 569

Supplementary Materials: The following supporting information can be downloaded at: www.mdpi.com/xxx/s1, Figure S1: Superposition of the EDA-AHR docking pose with the clusters obtained from the molecular dynamics of EDA with AHR.; Figure S2: Edaravone-induced expression of a xenobiotic responsive element (XRE)-driven reporter gene; Figure S3: Overlapping poses of the docking of GNF-351 with AHR; Figure S4: 2D representation of the bonds above 30% that GNF-351 makes with AHR during the 500 ns of molecular dynamics; Figure S5: Superimposing docking results and molecular dynamics of GNF-351 with AHR. Table S1: List of Taqman inventoried assays used for gene expression experiments; Spreadsheet S1: Raw transcriptomics data. 570 571 572 573 574 575 576 577 578

Author Contributions: Conceptualization, C.V., S.O., E.A., E.M. and C.A.; methodology, M.S.B., C.S., A.F., M.M., R.M. and M.C.M.; software, C.V. and S.O.; validation, C.V., E.M. and C.A.; formal analysis, C.V., S.O., M.S.B. and C.S.; investigation, C.V., S.O, E.M and C.A.; resources, C.V., S.O. and E.M. ; data curation, C.V., S.O., E.A., E.M and C.A.; writing—original draft preparation, C.A.; writing—review and editing, E.A., E.M. and C.A.; visualization, C.V., S.O., M.S.B., E.A. and E.M.; supervision, C.A.; project administration, C.A.; funding acquisition, E.M. and C.A. All authors have read and agreed to the published version of the manuscript. 579 580 581 582 583 584 585

Funding: This study was supported by FISM-Fondazione Italiana Sclerosi Multipla (grant cod. 2017/R/2 to CA), by intramural funding of Istituto Superiore di Sanità (Fasc. NEU23) and by the University of Padova to E.M. (PRID2021-MORO_BIRD2121_02). The funders had no role in study design, data collection and interpretation, or the decision to submit the work for publication. 586 587 588 589 590

Institutional Review Board Statement: The experimental procedures related to the use of CD1 Swiss mice were conducted following the Council Directive 86/609/EC and Decree 116/92 (Authorization n. 87/2017-PR - 09/23/2018 issued by the Service for Biotechnology and Animal Welfare of the "Istituto Superiore di Sanità" and by the Italian Ministry of Health. All procedures involving zebrafish embryos and larvae were performed according to the Italian Ministry of Health and the Local Institutional Review Board of the University of Padova (OPBA) (protocol code 312/2022-PR of 05/15/2022). 591 592 593 594 595 596 597

Data Availability Statement: All the data and simulations supporting the findings of this study are available from the corresponding author upon reasonable request. 598 599

Acknowledgments: The authors are grateful to Dr. Davide Murrau from the Institute for Genetic and Biomedical Research (IRGB), The National Research Council (CNR), Monserrato, Cagliari, Italy, for his technical and informatic support. 600 601 602

Conflicts of Interest: The authors declare no conflicts of interest. 603

References 604

1. Cho, H.; Shukla, S. Role of Edaravone as a Treatment Option for Patients with Amyotrophic Lateral Sclerosis. Pharmaceuticals 2020, 14, 29, doi:10.3390/ph14010029. 605 606
2. Michaličková, D.; Kübra Öztürk, H.; Hroudová, J.; Ľupták, M.; Kučera, T.; Hrnčíř, T.; Kutinová Canová, N.; Šíma, M.; Slanař, O. Edaravone Attenuates Disease Severity of Experimental Auto-Immune Encephalomyelitis and Increases Gene Expression of Nrf2 and HO-1. Physiol Res 2022, 147–157, doi:10.33549/physiolres.934800. 607 608 609
3. Bakhtiari, M.; Ghasemi, N.; Salehi, H.; Amirpour, N.; Kazemi, M.; Mardani, M. Evaluation of Edaravone Effects on the Differentiation of Human Adipose Derived Stem Cells into Oligodendrocyte Cells in Multiple Sclerosis Disease in Rats. Life Sciences 2021, 282, 119812, doi:10.1016/j.lfs.2021.119812. 610 611 612
4. Li, B.; Yu, D.; Xu, Z. Edaravone Prevents Neurotoxicity of Mutant L166P DJ-1 in Parkinson's Disease. J Mol Neurosci 2013, 51, 539–549, doi:10.1007/s12031-013-0022-8. 613 614
5. Liu, X.; Shao, R.; Li, M.; Yang, G. Edaravone Protects Neurons in the Rat Substantia Nigra Against 6-Hydroxydopamine-Induced Oxidative Stress Damage. Cell Biochem Biophys 2014, 70, 1247–1254, doi:10.1007/s12013-014-0048-8. 615 616
6. Jiao, S.-S.; Yao, X.-Q.; Liu, Y.-H.; Wang, Q.-H.; Zeng, F.; Lu, J.-J.; Liu, J.; Zhu, C.; Shen, L.-L.; Liu, C.-H.; et al. Edaravone Alleviates Alzheimer's Disease-Type Pathologies and Cognitive Deficits. Proc. Natl. Acad. Sci. U.S.A. 2015, 112, 5225–5230, doi:10.1073/pnas.1422998112. 617 618 619
7. Wang, X.; Zhou, L.; Chen, X.; Li, R.; Yu, B.; Pan, M.; Fang, L.; Li, J.; Cui, X.; Yao, M.; et al. Neuroprotective Effect and Possible Mechanism of Edaravone in Rat Models of Spinal Cord Injury: A Protocol for a Systematic Review and Meta-Analysis. Syst Rev 2023, 12, 177, doi:10.1186/s13643-023-02306-1. 620 621 622
8. Oosthoek, M.; Lili, A.; Almeida, A.; Van Loosbroek, O.; Van Der Geest, R.; De Greef-van Der Sandt, I.; Van Bokhoven, P.; Sikkes, S.A.M.; Teunissen, C.E.; Vijverberg, E.G.B. ASURE Clinical Trial Protocol: A Randomized, Placebo-Controlled, Proof-of-Concept Study Aiming to Evaluate Safety and Target Engagement Following Administration of TW001 in Early Alzheimer's Disease Patients. J Prev Alz Dis 2023, doi:10.14283/jpad.2023.107. 623 624 625 626
9. Watanabe, K.; Tanaka, M.; Yuki, S.; Hirai, M.; Yamamoto, Y. How Is Edaravone Effective against Acute Ischemic Stroke and Amyotrophic Lateral Sclerosis? J. Clin. Biochem. Nutr. 2018, 62, 20–38, doi:10.3164/jcbn.17-62. 627 628
10. Olufunmilayo, E.O.; Gerke-Duncan, M.B.; Holsinger, R.M.D. Oxidative Stress and Antioxidants in Neurodegenerative Disorders. Antioxidants 2023, 12, 517, doi:10.3390/antiox12020517. 629 630
11. Liu, Z.; Yang, C.; Meng, X.; Li, Z.; Lv, C.; Cao, P. Neuroprotection of Edaravone on the Hippocampus of Kainate-Induced Epilepsy Rats through Nrf2/HO-1 Pathway. Neurochemistry International 2018, 112, 159–165, doi:10.1016/j.neuint.2017.07.001. 631 632 633
12. Shou, L.; Bei, Y.; Song, Y.; Wang, L.; Ai, L.; Yan, Q.; He, W. Nrf2 Mediates the Protective Effect of Edaravone after Chlorpyrifos-induced Nervous System Toxicity. Environmental Toxicology 2019, 34, 626–633, doi:10.1002/tox.22728. 634 635
13. Zhang, L.; Guo, Y.; Wang, H.; Zhao, L.; Ma, Z.; Li, T.; Liu, J.; Sun, M.; Jian, Y.; Yao, L.; et al. Edaravone Reduces Aβ-Induced Oxidative Damage in SH-SY5Y Cells by Activating the Nrf2/ARE Signaling Pathway. Life Sciences 2019, 221, 259–266, doi:10.1016/j.lfs.2019.02.025. 636 637 638
14. Jangra, A.; Kwatra, M.; Singh, T.; Pant, R.; Kushwah, P.; Ahmed, S.; Dwivedi, D.; Saroha, B.; Lahkar, M. Edaravone Alleviates Cisplatin-Induced Neurobehavioral Deficits via Modulation of Oxidative Stress and Inflammatory Mediators in the Rat Hippocampus. European Journal of Pharmacology 2016, 791, 51–61, doi:10.1016/j.ejphar.2016.08.003. 639 640 641
15. Okuyama, S.; Morita, M.; Sawamoto, A.; Terugo, T.; Nakajima, M.; Furukawa, Y. Edaravone Enhances Brain-Derived Neurotrophic Factor Production in the Ischemic Mouse Brain. Pharmaceuticals 2015, 8, 176–185, doi:10.3390/ph8020176. 642 643
16. Ding, Y.; Zhu, W.; Kong, W.; Li, T.; Zou, P.; Chen, H. Edaravone Attenuates Neuronal Apoptosis in Hippocampus of Rat Traumatic Brain Injury Model via Activation of BDNF/TrkB Signaling Pathway. Arch Med Sci 2021, 17, 514–522, doi:10.5114/aoms.2019.89849. 644 645 646
17. Yang, Y.; Yi, J.; Pan, M.; Hu, B.; Duan, H. Edaravone Alleviated Propofol-Induced Neural Injury in Developing Rats by BDNF/TrkB Pathway. J Cell Mol Med 2021, 25, 4974–4987, doi:10.1111/jcmm.16422. 647 648
18. Wu, H.-T.; Yu, Y.; Li, X.-X.; Lang, X.-Y.; Gu, R.-Z.; Fan, S.-R.; Fang, X.; Bai, J.-P.; Lan, R.; Qin, X.-Y. Edaravone Attenuates H2O2 or Glutamate-Induced Toxicity in Hippocampal Neurons and Improves AlCl3/D-Galactose Induced Cognitive Impairment in Mice. NeuroToxicology 2021, 85, 68–78, doi:10.1016/j.neuro.2021.05.005. 649 650 651

19. Eleuteri, C.; Olla, S.; Veroni, C.; Umeton, R.; Mechelli, R.; Romano, S.; Buscarinu, Mc.; Ferrari, F.; Calò, G.; Ristori, G.; et al. A Staged Screening of Registered Drugs Highlights Remyelinating Drug Candidates for Clinical Trials. Sci Rep 2017, 7, 45780, doi:10.1038/srep45780. 652 653 654
20. Takase, H.; Liang, A.C.; Miyamoto, N.; Hamanaka, G.; Ohtomo, R.; Maki, T.; Pham, L.-D.D.; Lok, J.; Lo, E.H.; Arai, K. Protective Effects of a Radical Scavenger Edaravone on Oligodendrocyte Precursor Cells against Oxidative Stress. Neuroscience Letters 2018, 668, 120–125, doi:10.1016/j.neulet.2018.01.018. 655 656 657
21. Luo, W.; Xu, H.; Xu, L.; Jiang, W.; Chen, C.; Chang, Y.; Liu, C.; Tian, Z.; Qiu, X.; Xie, C.; et al. Remyelination in Neuromyelitis Optica Spectrum Disorder Is Promoted by Edaravone through MTORC1 Signaling Activation. Glia 2023, 71, 284–304, doi:10.1002/glia.24271. 658 659 660
22. Colombo, E.; Olla, S.; Minnelli, C.; Formato, A.; Veroni, C.; Corbisiero, S.; Pericolo, M.; Siguri, C.; Mobbili, G.; Agresti, C.; et al. Synthesis and Characterization of Edaravone Analogues as Remyelinating Agents and Putative Mechanistic Probes. Molecules 2023, 28, 6928, doi:10.3390/molecules28196928. 661 662 663
23. Agresti, C.; D'Urso, D.; Levi, G. Reversible Inhibitory Effects of Interferon-Gamma and Tumour Necrosis Factor-Alpha on Oligodendroglial Lineage Cell Proliferation and Differentiation in Vitro. Eur J Neurosci 1996, 8, 1106–1116, doi:10.1111/j.1460-9568.1996.tb01278.x. 664 665 666
24. Gruszczyk, J.; Grandvuillemin, L.; Lai-Kee-Him, J.; Paloni, M.; Savva, C.G.; Germain, P.; Grimaldi, M.; Boulahtouf, A.; Kwong, H.-S.; Bous, J.; et al. Cryo-EM Structure of the Agonist-Bound Hsp90-XAP2-AHR Cytosolic Complex. Nat Commun 2022, 13, 7010, doi:10.1038/s41467-022-34773-w. 667 668 669
25. Lu, C.; Wu, C.; Ghoreishi, D.; Chen, W.; Wang, L.; Damm, W.; Ross, G.A.; Dahlgren, M.K.; Russell, E.; Von Bargen, C.D.; et al. OPLS4: Improving Force Field Accuracy on Challenging Regimes of Chemical Space. J. Chem. Theory Comput. 2021, 17, 4291–4300, doi:10.1021/acs.jctc.1c00302. 670 671 672
26. Friesner, R.A.; Banks, J.L.; Murphy, R.B.; Halgren, T.A.; Klicic, J.J.; Mainz, D.T.; Repasky, M.P.; Knoll, E.H.; Shelley, M.; Perry, J.K.; et al. Glide: A New Approach for Rapid, Accurate Docking and Scoring. 1. Method and Assessment of Docking Accuracy. J. Med. Chem. 2004, 47, 1739–1749, doi:10.1021/jm0306430. 673 674 675
27. Halgren, T.A.; Murphy, R.B.; Friesner, R.A.; Beard, H.S.; Frye, L.L.; Pollard, W.T.; Banks, J.L. Glide: A New Approach for Rapid, Accurate Docking and Scoring. 2. Enrichment Factors in Database Screening. J. Med. Chem. 2004, 47, 1750–1759, doi:10.1021/jm030644s. 676 677 678
28. Banks, J.L.; Beard, H.S.; Cao, Y.; Cho, A.E.; Damm, W.; Farid, R.; Felts, A.K.; Halgren, T.A.; Mainz, D.T.; Maple, J.R.; et al. Integrated Modeling Program, Applied Chemical Theory (IMPACT). J Comput Chem 2005, 26, 1752–1780, doi:10.1002/jcc.20292. 679 680 681
29. Friesner, R.A.; Murphy, R.B.; Repasky, M.P.; Frye, L.L.; Greenwood, J.R.; Halgren, T.A.; Sanschagrin, P.C.; Mainz, D.T. Extra Precision Glide: Docking and Scoring Incorporating a Model of Hydrophobic Enclosure for Protein−Ligand Complexes. J. Med. Chem. 2006, 49, 6177–6196, doi:10.1021/jm051256o. 682 683 684
30. Genheden, S.; Ryde, U. The MM/PBSA and MM/GBSA Methods to Estimate Ligand-Binding Affinities. Expert Opinion on Drug Discovery 2015, 10, 449–461, doi:10.1517/17460441.2015.1032936. 685 686
31. Li, J.; Abel, R.; Zhu, K.; Cao, Y.; Zhao, S.; Friesner, R.A. The VSGB 2.0 Model: A next Generation Energy Model for High Resolution Protein Structure Modeling. Proteins 2011, 79, 2794–2812, doi:10.1002/prot.23106. 687 688
32. Morris, G.M.; Huey, R.; Lindstrom, W.; Sanner, M.F.; Belew, R.K.; Goodsell, D.S.; Olson, A.J. AutoDock4 and AutoDockTools4: Automated Docking with Selective Receptor Flexibility. J Comput Chem 2009, 30, 2785–2791, doi:10.1002/jcc.21256. 689 690 691
33. Gasteiger, J.; Marsili, M. A New Model for Calculating Atomic Charges in Molecules. Tetrahedron Letters 1978, 19, 3181–3184, doi:10.1016/S0040-4039(01)94977-9. 692 693
34. Sallem, M.A.S.; Sousa, S.A.J.D. AutoGrid: Towards an Autonomic Grid Middleware. In Proceedings of the 16th IEEE International Workshops on Enabling Technologies: Infrastructure for Collaborative Enterprises (WETICE 2007); IEEE: Evry Cedex, France, 2007; pp. 223–228. 694 695 696
35. Moitessier, N.; Englebienne, P.; Lee, D.; Lawandi, J.; Corbeil, C.R. Towards the Development of Universal, Fast and Highly Accurate Docking/Scoring Methods: A Long Way to Go. British J Pharmacology 2008, 153, doi:10.1038/sj.bjp.0707515. 697 698
36. Meng, X.-Y.; Zhang, H.-X.; Mezei, M.; Cui, M. Molecular Docking: A Powerful Approach for Structure-Based Drug Discovery. CAD 2011, 7, 146–157, doi:10.2174/157340911795677602. 699 700
37. Bowers, K.J.; Chow, D.E.; Xu, H.; Dror, R.O.; Eastwood, M.P.; Gregersen, B.A.; Klepeis, J.L.; Kolossvary, I.; Moraes, M.A.; Sacerdoti, F.D.; et al. Scalable Algorithms for Molecular Dynamics Simulations on Commodity Clusters. In Proceedings of the ACM/IEEE SC 2006 Conference (SC'06); IEEE: Tampa, FL, November 2006; pp. 43–43. 701 702 703
38. Jorgensen, W.L.; Chandrasekhar, J.; Madura, J.D.; Impey, R.W.; Klein, M.L. Comparison of Simple Potential Functions for Simulating Liquid Water. The Journal of Chemical Physics 1983, 79, 926–935, doi:10.1063/1.445869. 704 705
39. Hoover, W.G. Canonical Dynamics: Equilibrium Phase-Space Distributions. Phys. Rev. A 1985, 31, 1695–1697, doi:10.1103/PhysRevA.31.16. 706 707
40. Martyna, G.J.; Tobias, D.J.; Klein, M.L. Constant Pressure Molecular Dynamics Algorithms. The Journal of Chemical Physics 1994, 101, 4177–4189, doi:10.1063/1.467468. 708 709

41. Frey, B.J.; Dueck, D. Clustering by Passing Messages Between Data Points. Science 2007, 315, 972–976, doi:10.1126/science.1136800. 710 711
42. Mallozzi, C.; Pepponi, R.; Visentin, S.; Chiodi, V.; Lombroso, P.J.; Bader, M.; Popoli, P.; Domenici, M.R. The Activity of the Striatal-enriched Protein Tyrosine Phosphatase in Neuronal Cells Is Modulated by Adenosine A 2A Receptor. Journal of Neurochemistry 2020, 152, 284–298, doi:10.1111/jnc.14866. 712 713 714
43. Morel, Y.; Mermod, N.; Barouki, R. An Autoregulatory Loop Controlling CYP1A1 Gene Expression: Role of H 2 O 2 and NFI. Molecular and Cellular Biology 1999, 19, 6825–6832, doi:10.1128/MCB.19.10.6825. 715 716
44. Nebert, D.W.; Dalton, T.P.; Okey, A.B.; Gonzalez, F.J. Role of Aryl Hydrocarbon Receptor-Mediated Induction of the CYP1 Enzymes in Environmental Toxicity and Cancer. Journal of Biological Chemistry 2004, 279, 23847–23850, doi:10.1074/jbc.R400004200. 717 718 719
45. Imran, S.; Ferretti, P.; Vrzal, R. Different Regulation of Aryl Hydrocarbon Receptor-Regulated Genes in Response to Dioxin in Undifferentiated and Neuronally Differentiated Human Neuroblastoma SH-SY5Y Cells. Toxicology Mechanisms and Methods 2015, 25, 689–697, doi:10.3109/15376516.2015.1070227. 720 721 722
46. Miao, W.; Hu, L.; Scrivens, P.J.; Batist, G. Transcriptional Regulation of NF-E2 P45-Related Factor (NRF2) Expression by the Aryl Hydrocarbon Receptor-Xenobiotic Response Element Signaling Pathway. Journal of Biological Chemistry 2005, 280, 20340–20348, doi:10.1074/jbc.M412081200. 723 724 725
47. Badenetti, L.; Manzoli, R.; Rubin, M.; Cozza, G.; Moro, E. Monitoring Nrf2/ARE Pathway Activity with a New Zebrafish Reporter System. IJMS 2023, 24, 6804, doi:10.3390/ijms24076804. 726 727
48. Sekhar, K.R.; Crooks, P.A.; Sonar, V.N.; Friedman, D.B.; Chan, J.Y.; Meredith, M.J.; Starnes, J.H.; Kelton, K.R.; Summar, S.R.; Sasi, S.; et al. NADPH Oxidase Activity Is Essential for Keap1/Nrf2-Mediated Induction of GCLC in Response to 2-Indol-3-Yl-Methylenequinuclidin-3-Ols. Cancer Res 2003, 63, 5636–5645. 728 729 730
49. Shackleford, G.; Sampathkumar, N.K.; Hichor, M.; Weill, L.; Meffre, D.; Juricek, L.; Laurendeau, I.; Chevallier, A.; Ortonne, N.; Larousserie, F.; et al. Involvement of Aryl Hydrocarbon Receptor in Myelination and in Human Nerve Sheath Tumorigenesis. Proc. Natl. Acad. Sci. U.S.A. 2018, 115, doi:10.1073/pnas.1715999115. 731 732 733
50. Nellessen, A.; Nyamoya, S.; Zendedel, A.; Slowik, A.; Wruck, C.; Beyer, C.; Fragoulis, A.; Clarner, T. Nrf2 Deficiency Increases Oligodendrocyte Loss, Demyelination, Neuroinflammation and Axonal Damage in an MS Animal Model. Metab Brain Dis 2020, 35, 353–362, doi:10.1007/s11011-019-00488-z. 734 735 736
51. Shin, J.; Park, H.-C.; Topczewska, J.M.; Mawdsley, D.J.; Appel, B. Neural Cell Fate Analysis in Zebrafish Using Olig2 BAC Transgenics. Methods Cell Sci 2003, 25, 7–14, doi:10.1023/B:MICS.0000006847.09037.3a. 737 738
52. Smith, K.J.; Murray, I.A.; Tanos, R.; Tellew, J.; Boitano, A.E.; Bisson, W.H.; Kolluri, S.K.; Cooke, M.P.; Perdew, G.H. Identification of a High-Affinity Ligand That Exhibits Complete Aryl Hydrocarbon Receptor Antagonism. J Pharmacol Exp Ther 2011, 338, 318–327, doi:10.1124/jpet.110.178392. 739 740 741
53. Avilla, M.N.; Malecki, K.M.C.; Hahn, M.E.; Wilson, R.H.; Bradfield, C.A. The Ah Receptor: Adaptive Metabolism, Ligand Diversity, and the Xenokine Model. Chem. Res. Toxicol. 2020, 33, 860–879, doi:10.1021/acs.chemrestox.9b00476. 742 743
54. Rothhammer, V.; Quintana, F.J. The Aryl Hydrocarbon Receptor: An Environmental Sensor Integrating Immune Responses in Health and Disease. Nat Rev Immunol 2019, 19, 184–197, doi:10.1038/s41577-019-0125-8. 744 745
55. Ye, W.; Chen, R.; Chen, X.; Huang, B.; Lin, R.; Xie, X.; Chen, J.; Jiang, J.; Deng, Y.; Wen, J. AhR Regulates the Expression of Human Cytochrome P450 1A1 (CYP1A1) by Recruiting Sp1. The FEBS Journal 2019, 286, 4215–4231, doi:10.1111/febs.14956. 746 747
56. Großkopf, H.; Walter, K.; Karkossa, I.; Von Bergen, M.; Schubert, K. Non-Genomic AhR-Signaling Modulates the Immune Response in Endotoxin-Activated Macrophages After Activation by the Environmental Stressor BaP. Front. Immunol. 2021, 12, 620270, doi:10.3389/fimmu.2021.620270. 748 749 750
57. Stading, R.; Chu, C.; Couroucli, X.; Lingappan, K.; Moorthy, B. Molecular Role of Cytochrome P4501A Enzymes in Oxidative Stress. Current Opinion in Toxicology 2020, 20–21, 77–84, doi:10.1016/j.cotox.2020.07.001. 751 752
58. Wang, G.; Zeng, X.; Gong, S.; Wang, S.; Ge, A.; Liu, W.; Ge, J.; He, Q. Exploring the Mechanism of Edaravone for Oxidative Stress in Rats with Cerebral Infarction Based on Quantitative Proteomics Technology. Evid Based Complement Alternat Med 2022, 2022, 8653697, doi:10.1155/2022/8653697. 753 754 755
59. Martin, N.R.; Patel, R.; Kossack, M.E.; Tian, L.; Camarillo, M.A.; Cintrón-Rivera, L.G.; Gawdzik, J.C.; Yue, M.S.; Nwagugo, F.O.; Elemans, L.M.H.; et al. Proper Modulation of AHR Signaling Is Necessary for Establishing Neural Connectivity and Oligodendrocyte Precursor Cell Development in the Embryonic Zebrafish Brain. Front. Mol. Neurosci. 2022, 15, 1032302, doi:10.3389/fnmol.2022.1032302. 756 757 758 759
60. Juricek, L.; Carcaud, J.; Pelhaitre, A.; Riday, T.T.; Chevallier, A.; Lanzini, J.; Auzeil, N.; Laprévote, O.; Dumont, F.; Jacques, S.; et al. AhR-Deficiency as a Cause of Demyelinating Disease and Inflammation. Sci Rep 2017, 7, 9794, doi:10.1038/s41598-017-09621-3. 760 761 762
61. Majumder, S.; Kono, M.; Lee, Y.T.; Byrnes, C.; Li, C.; Tuymetova, G.; Proia, R.L. A Genome-Wide CRISPR/Cas9 Screen Reveals That the Aryl Hydrocarbon Receptor Stimulates Sphingolipid Levels. Journal of Biological Chemistry 2020, 295, 4341–4349, doi:10.1074/jbc.AC119.011170. 763 764 765
62. Grishanova, A.Y.; Perepechaeva, M.L. Aryl Hydrocarbon Receptor in Oxidative Stress as a Double Agent and Its Biological and Therapeutic Significance. IJMS 2022, 23, 6719, doi:10.3390/ijms23126719. 766 767

63. Tsaktanis, T.; Beyer, T.; Nirschl, L.; Linnerbauer, M.; Grummel, V.; Bussas, M.; Tjon, E.; Mühlau, M.; Korn, T.; Hemmer, B.; et al. Aryl Hydrocarbon Receptor Plasma Agonist Activity Correlates With Disease Activity in Progressive MS. Neurol Neuroimmunol Neuroinflamm 2021, 8, e933, doi:10.1212/NXI.0000000000000933.
64. Rothhammer, V.; Kenison, J.E.; Li, Z.; Tjon, E.; Takenaka, M.C.; Chao, C.-C.; Alves De Lima, K.; Borucki, D.M.; Kaye, J.; Quintana, F.J. Aryl Hydrocarbon Receptor Activation in Astrocytes by Laquinimod Ameliorates Autoimmune Inflammation in the CNS. Neurol Neuroimmunol Neuroinflamm 2021, 8, e946, doi:10.1212/NXI.0000000000000946.
65. O'Donnell, E.F.; Saili, K.S.; Koch, D.C.; Kopparapu, P.R.; Farrer, D.; Bisson, W.H.; Mathew, L.K.; Sengupta, S.; Kerkvliet, N.I.; Tanguay, R.L.; et al. The Anti-Inflammatory Drug Leflunomide Is an Agonist of the Aryl Hydrocarbon Receptor. PLoS ONE 2010, 5, e13128, doi:10.1371/journal.pone.0013128.

Disclaimer/Publisher's Note: The statements, opinions and data contained in all publications are solely those of the individual author(s) and contributor(s) and not of MDPI and/or the editor(s). MDPI and/or the editor(s) disclaim responsibility for any injury to people or property resulting from any ideas, methods, instructions or products referred to in the content.